ANALYTICAL STUDY OF A HIGH-RESOLUTION POSITRON RING DETECTOR SYSTEM FOR TRANSAXIAL RECONSTRUCTION TOMOGRAPHY

Stephen E. Derenzo, Haim Zaklad, and Thomas F. Budinger

Lawrence Berkeley Laboratory, University of California, Berkeley, California

This paper presents an analytical study of a high-resolution positron ring detector system for transaxial reconstruction tomography. Our goal is a combination of good spatial resolution, high sensitivity, rejection of scattered photons, variable section thickness, and the minimization of the number of photomultipliers and coincidence circuits. A circular ring of 288 NaI(Tl) crystals 0.8 cm wide should provide a resolution of 4–7 mm FWHM over a circular region 30 cm in diameter. Coded light pipes permit readout using only 72 photomultipliers and 12 coincidence circuits. With properly designed shielding and an energy resolution of 30% FWHM, a positron activity of 200 μCi per axial centimeter in a 20-cm-diam cylinder of tissue should provide approximately 7,000 events/sec from a 2-cm-thick transaxial section (including a 5% accidental coincident background and a 26% scattered coincident background). This rate is adequate for both static and dynamic imaging. The device can operate at two to three times higher event rates with increased backgrounds.

A clear and valuable goal in nuclear medicine is the rapid, quantitative, three-dimensional imaging of radionuclide distributions within the human body. One realization of this goal is the use of positron-emitting pharmaceuticals coupled with a ring of detectors completely surrounding the body (*1–4*). The following are some factors that make this approach timely and attractive. (A) Coincident detection of back-to-back annihilation radiation exploits a much larger solid angle than single gamma imaging, resulting in a great increase in imaging efficiency. (B) The use of a ring of detectors shielded from activity external to the section being imaged provides discrimination against gamma rays scattered in the patient. (C) A large ring of closely packed detectors can provide a sufficiently large number of viewing angles to eliminate the need to rotate the detector system or the patient during exposure. (D) In recent years much progress has been made in the mathematical techniques of computerized transaxial tomography (*5,6*). This, coupled with the fact that attenuation corrections are easily made for the coincident detection of annihilation radiation, gives us the potential for the quantitative determination of the distribution of activity on a microcurie per cubic centimeter basis. And (E) in recent years progress has also been made in the production and availability of positron-emitting isotopes [e.g., cyclotron-produced 20-min ^{11}C, 10-min ^{13}N, 2-min ^{15}O, 1.8-hr ^{18}F, 4.6-hr ^{81}Rb, 9-hr ^{52}Fe, and 9-hr ^{62}Zn; and generator-produced 68-min ^{68}Ga (from 280-day ^{68}Ge) and 1.3-min ^{82}Rb (from 25-day ^{82}Sr)]. A few of the many references to clinical applications of such emitters may be found in Refs. *7* and *8*. In addition, many other positron-emitting pharmaceuticals are being developed for nuclear medicine (*9*).

BACKGROUND

The application of positron detection in nuclear medicine was suggested in the early 1950s by Wrenn and coworkers (*10*) and by Brownell and Sweet (*11*). Later, Anger presented a positron-imaging system using a scintillation camera in coincidence with a crystal array (*12*). Use of this device in clinical medicine has been limited by inadequate speed, resulting in saturation at counting rates of ~1000/sec in tissue. This limitation has been overcome in part by the MGH camera, which employs two parallel rectangular detector arrays each having 127

Received April 8, 1975; revision accepted Aug. 18, 1975.

For reprints contact: S. E. Derenzo, Donner Laboratory, University of California, Berkeley, Calif. 94720.

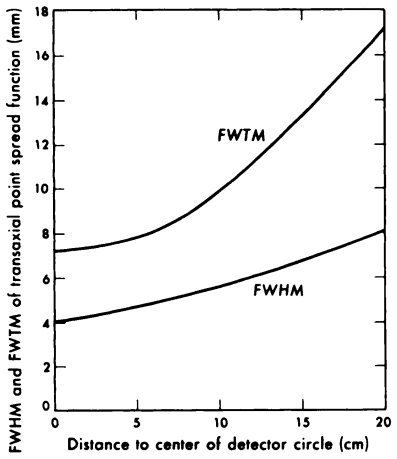

FIG. 1. Full width at half maximum (FWHM) and full width at one-tenth maximum (FWTM) of transaxial point spread function (averaged over all photon directions) vs distance to center of detector circle. Detector ring is assumed to be 80 cm in diameter and composed of 288 NaI(Tl) crystals each 8 mm wide.

NaI(Tl) crystals and 72 photomultipliers (*13*). The resolution is 10 mm FWHM and counting rates of 10,000/sec are possible in 20-cm water. A two-plane positron camera system employing lead converters and multiwire chambers is being evaluated at the University of California San Francisco Medical Center (*14*). The resolution is 7 mm FWHM but the maximum counting rate is currently limited to 120/sec in 10-cm Plexiglas. Another two-plane positron camera system employing two Anger scintillation cameras is being developed at Searle Radiographics (*15*).The resolution is 10 mm FWHM and counting rates in excess of 4,000/sec are possible in 12-cm water. Efficient transaxial tomography using these systems involves patient or detector rotation, and dynamic flow studies are not possible except indirectly through use of the equilibrium image method (*16*).

The concept of a ring detector system was introduced in 1962 by a group at Brookhaven National Laboratory who used coincident positron detection for transaxial tomographic imaging (*1*). The device consists of 32 NaI(Tl) crystals. Mathematical techniques capable of solving the image reconstruction problem were not employed until recently (*2*). Phelps, Ter-Pogossian, and coworkers reported on a similar device with a resolution of 11 mm FWHM using 24 NaI(Tl) detectors in a hexagonal pattern (*3,4*). A 48-detector system, large enough for human use, has been constructed and is now being tested. Work is also in progress at UCLA to build a 64-crystal positron ring system with an anticipated resolution of 10 mm FWHM (*17*).

In this paper we present the results of a design study on positron ring detectors for transaxial tomography. Our analysis is based on the goal of achieving a combination of good spatial resolution, high sensitivity, rejection of photons that scatter in the tissue or in the detector, variable section thickness, and economic feasibility. This is the first report of a coded light-pipe scheme for a ring of detectors.

SPATIAL RESOLUTION

One means of realizing good spatial resolution is by using a large number of small crystals. For example, for an 80-cm-diam ring of NaI(Tl) crystals, each 0.8 cm wide and 5 cm deep, and an energy threshold of 410 keV, the resolution is 4 mm FWHM at the center of the ring and 6.5 mm FWHM at a distance of 15 cm from the center of the ring (Fig. 1). Resolution deteriorates with increasing distance from the ring axis because of the increase in the apparent size of the crystals (Fig. 2). (For a detailed analysis see Ref. *18*.) For this detector ring of 288 crystals it is difficult to couple each crystal optically to a photomultiplier tube (PMT) because of the large number of crystals and the close physical packing.

This problem can be overcome by dividing the detector ring into segments and optically coupling each crystal to several PMTs using a code that uniquely specifies its position within the segment (*19*). An example of such a code for six crystals and four PMTs is shown in Fig. 3. Each crystal is optically coupled to two PMTs by light pipes and each light pipe corresponds to a logic ONE in the truth table. When a crystal scintillates, its digital position code is directly available by interrogating the output of the PMTs.

By representing each crystal with the same number of logic ONEs it is possible to reject events where a significant amount of energy has been deposited in more than one crystal of a segment, since in such cases more than the prescribed number of PMTs will respond. This can occur when a photon

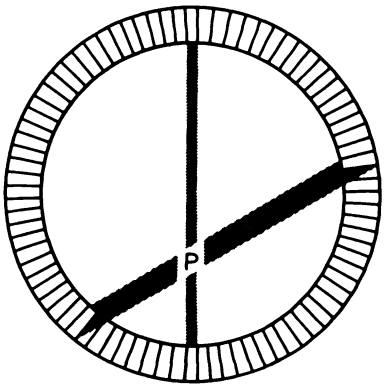

FIG. 2. Detector ring and source (P) showing that for off-axis points transaxial resolution depends on photon direction.

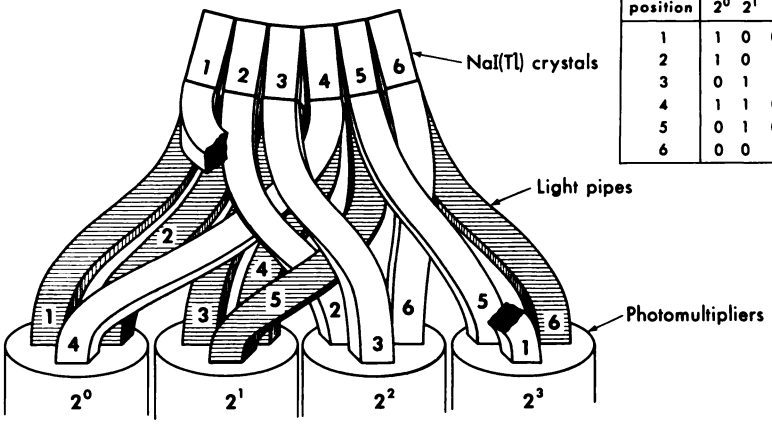

Light Pipe Connection Scheme

Crystal position	PMT 2^0	2^1	2^2	2^3
1	1	0	0	1
2	1	0	1	0
3	0	1	1	0
4	1	1	0	0
5	0	1	0	1
6	0	0	1	1

FIG. 3. Example showing coding scheme for four photomultipliers and six crystals. In table "one" represents light-pipe connection between crystal and PMT. Expansion of 36 crystals requires 60 additional light pipes and 5 additional photomultipliers.

scatters in the crystals or when two photons are detected in the same segment within the coincidence resolving time.

In general, the maximum number of distinct combinations is given by

$$\frac{n!}{m!\,(n-m)!}$$

where n is the number of PMTs serving each segment and m is the number of PMTs to which each crystal is coupled. In the example of Fig. 3 the code for a segment containing six crystals used $n = 4$ and $m = 2$.

The number of PMTs is minimized when $m \approx n/2$, while the number of light pipes is minimized when m is small. The use of binary and Gray codes will reduce the number of PMTs somewhat further but will not permit the rejection of multiple detections. The fast digital coding of crystal positions allows each segment to be placed in coincidence with several opposing segments at high rates using a small number of coincidence circuits. Then crystal address codes can be compared to place each crystal in coincidence with a predetermined number of opposing crystals.

In the case of 8 segments of 36 crystals each, the choice of $n = 9$ and $m = 2$ allows 72 PMTs to serve 288 crystals by 576 light pipes and 12 coincidence circuits.

ENERGY AND TIME RESOLUTION

The energy resolution of a scintillation detector depends on the amount of scintillation light produced, the light-collection efficiency, and the quantum efficiency of the PMT at the relevant wavelengths. A NaI(Tl) crystal 5 cm diam × 5 cm can achieve an energy resolution of 8% FWHM for 511-keV photons, but any reduction in the light reaching the PMT (such as through the use of narrow crystals or by coupling the crystal to the PMT by a long light pipe) will degrade the resolution.

Grenier, et al report an energy resolution of 23% FWHM at 122 keV and 10% FWHM at 662 keV for a 9 × 9 × 38-mm NaI(Tl) crystal coupled directly to a PMT; and a resolution of 50% at 122 keV when the same crystal was coupled to the PMT by a 61-cm-long plastic light pipe that transmitted 20% of the full-energy light (*20*). Their data show, as expected, that the width of the full-energy peak is inversely proportional to the square root of the number of photons reaching PMT. Since the crystals listed in the example of Table 1 are similar in size and would be coupled to the PMTs by similar light pipes, we expect that at 511 keV the energy resolution will be approximately 50% FWHM $\times \sqrt{122\text{ keV}/511\text{ keV}} = 24\%$ FWHM. Any nonuniformity among the light pipes will result in a further degradation of the resolution.

The time resolution in NaI(Tl) depends on the same statistical fluctuations that determine the energy resolution. Braunsfurth, et al report a time-jitter distribution with a FWHM of 1.3 nsec for 511-keV photon pairs in NaI(Tl), using a system with a good light-collection efficiency (*21*). We expect that the time-jitter distribution of a ring detector system with an energy resolution of 24% FWHM will have a FWHM of 1.3 nsec × (24%/8%) = 3.9 nsec. A 10-nsec coincidence resolving time is assumed in Table 1.

SENSITIVITY

The event rate for the simultaneous detection of two annihilation photons may be calculated as the following product: (contributing activity) × (probability of photon No. 1 reaching a detector) × (probability of photon No. 2 reaching a detector)

TABLE 1. PROPERTIES OF A RING DETECTOR SYSTEM* FOR THREE ASSUMED ENERGY RESOLUTIONS

Quantity	Symbol	Units	Case 1	Case 2	Case 3
Energy resolution (FWHM) at 511 keV	Γ	%	none	30	15
Energy threshold	E_p	keV	100	410†‡	460†‡
Approximate maximum scattering angle corresponding to E_p (Eq. 3)	θ_p	degrees	180	41	27
Effective maximum scattering angle	θ_m	degrees	40	40	27
Minimum scattered gamma energy corresponding to θ_m (Eq. 4)	E_m	keV	415	415	460
Average detection efficiency for photon energies from E_m to 511 keV	ϵ_m	%	65	48	45
Detection efficiency for 511-keV gammas	ϵ	%	53	43	43
Probability that 511-keV gamma will scatter and retain an energy above E_p (Eq. 9)	P_p	%	63	20	10
Average detection efficiency for gamma energies from E_p to 511 keV	ϵ_p	%	80	48	45
Geometry factor—one gamma scatters (Eq. 6)	g_1	—	0.31	0.31	0.23
Geometry factor—both gammas scatter	g_2	—	0.19	0.19	0.13
Rate for unscattered coincident events (Eq. 1)	C_o	events per sec	7,100	4,700	4,700
Sensitivity	C_o/ρ	events per sec per [μCi/cm]	36	23	23
Rate for scattered coincident events (Eqs. 5 and 7)	$C_1 + C_2$	events per sec	3,020	1,740	1,160
Singles rate for entire ring (Eq. 8)	C_s	10^5 events per sec	10.4	3.8	3.0
Accidental coincidence rate for entire ring (Eq. 10)	C_a	events per sec	2,400	320	200
Total event rate ($C_o + C_1 + C_2 + C_a$)		events per sec	12,520	6,760	6,060
Background fraction $\frac{C_1 + C_2 + C_a}{C_o + C_1 + C_2 + C_a}$		%	43	30	22
Paralyzing deadtime	t_p	nsec	200	800	800
Fraction of events lost due to deadtime (Eq. 13)	f_o	%	5‡	23‡	23‡

* Physical specifications of assumed ring detector system are as follows: c = detector ring radius = 40 cm, S = shielding slit width = 2 cm, T = shielding slit depth = 20 cm, P_s = probability of scattering on emerging from the center of 20-cm-diam cylinder of water = 63%, f = 0.22 (for 288 crystals, each would be in coincidence with opposing 62 crystals), $\theta_t = 40°$ maximum scattering angle imposed by coincidence requirement (approximate), ρ = activity density = 200 μCi/axial cm, t = time resolution = 10 nsec, dimension of crystals along gamma line of flight = 5 cm, dimension of crystals along ring axis = 3 cm, dimension of crystals transverse to ring axis = 0.8 cm, R = radius of uniform geometric sensitivity = 14 cm, and G = gross singles rate per segment = 1.3×10^5 counts/sec.

† Corresponds to 7% photopeak loss, assuming that the photopeak has Gaussian distribution.

‡ This event loss has not been included elsewhere in this table.

$\times$ (product of detector efficiencies). This formulation is used below for both unscattered (Eq. 1) and scattered (Eqs. 5 and 7) photons.

The unscattered coincident event rate C_o of a ring detector is approximated by:

$$C_o = \left[\frac{\rho a S}{2}\right]\left[\frac{S\, e^{-\mu L}}{2c}\right]\left[\epsilon^2\right] = \left[\frac{\rho a S^2\, e^{-\mu L}\, \epsilon^2}{4c}\right], \quad (1)$$

where ρ is the activity density in microcuries per axial centimeter, a is the 37,000 annihilations per second per microcurie of β^+ (conversion factor), S is the exposed dimension of detector ring along ring axis (determined by width of shielding slit—see Fig. 4), $e^{-\mu L}$ is the probability that neither photon scatters in the tissue, μ is the narrow-beam attenuation coefficient for 511-keV photons in tissue (in water μ = 0.10 cm^{-1}), L is the tissue thickness, c is the radius of detector ring, and ϵ is the detection efficiency for 511-keV photons. The first bracket is the contributing activity; the second bracket is the probability that both photons reach the detector ring without having scattered; and the third bracket is the probability that both photons are detected and pass the pulse-height threshold.

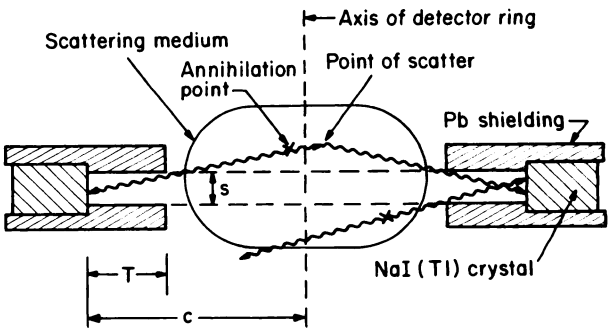

FIG. 4. Illustration showing how Compton scattering can contribute background to coincident event rate. Although two photons are in time coincidence, they are not colinear and provide erroneous spatial information. Unscattered coincident events can arise only from region between dashed lines.

We assume that the source distribution lies within a distance R from the ring axis given by:

$$R = c \sin(f\pi/2), \quad (2)$$

where each detector (of a total of N) is in coincidence with the fN opposing detectors. For a circular ring the geometric sensitivity is nearly uniform within the radius R. We also assume that the detectors are densely packed around the ring and that the shielding blocks only photons external to the section being imaged.

In Table 1 we have calculated the sensitivity C_o/ρ and many other parameters for a particular positron ring detector system and a tissue thickness of 20 cm ($\mu L = 2$). In this example the event rate is 5,000–7,000 events/sec for $\rho = 200$ μCi/axial cm. Thus if the section is to be resolved into a grid of 40 × 40 pictels, 300–400 events can be collected per pictel over a 100-sec time period. Let us also consider the case of gated imaging of the myocardium using generator-produced 75-sec ^{82}Rb. We assume that (A) the heart is 10 cm in the cephalad–caudad dimension and the myocardial volume is 150 cm^3; (B) the cardiac rate is 72/min; (C) the scattering medium is equivalent to a 20-cm-diam cylinder of water; (D) 20 mCi of ^{82}Rb is injected i.v. and 3.5% of this is extracted by the myocardium; (E) eight separate images are taken, each corresponding to a 0.1-sec interval of the 0.8-sec cardiac cycle; (F) data are taken for a period of 200 sec after an initial 100-sec wait for the blood pool clearance of ^{82}Rb; and (G) as in Table 1, Case 2, the imaging sensitivity is 23 events/sec [μCi per axial cm]$^{-1}$. The resulting initial activity density is 0.7 μCi per image element (4 × 4 × 10 mm) and for each of the eight images typically 90 events will be collected per image element.

The greater imaging sensitivity of the positron ring detector over conventional single gamma imaging arises primarily from a greater solid angle. The ring detector has a solid-angle factor of S/2c which is 0.025 for the example of Table 1. In single gamma imaging only a small area of the crystal ($\sim\pi d^2/4$ for a resolution distance d) receives photons from sources at a typical imaging distance D. For low photon energy the resulting solid-angle factor is approximately $(\pi d^2/4)/(4\pi D^2) = 4.5 \times 10^{-5}$ for d = 4 mm and D = 15 cm. Thus in these examples the positron ring detector has a solid angle approximately 500 times greater than with gamma imaging, with the additional benefit of transaxial tomography without rotation.

SHIELDING AND BACKGROUNDS

Shielding is essential for blocking radiation emitted by activity external to the section being imaged. Furthermore, varying the width of the shielding slit allows the section thickness to be varied. True unscattered coincident events can arise only from a positron activity $\rho S/2$ within the section, but scattered coincident events and single counts (both of which contribute to the background) can arise from an activity that is effectively $\rho cS/T$, where T is the depth of the shielding slit (Fig. 4).

There are two methods available for rejecting scattered photons. The coincidence requirement (i.e., that each of the N detectors be in coincidence with the fN opposing detectors) establishes an approximate upper limit $\theta_f = f\pi$ on the scattering angle. This approximation is realistic since the size of the scattering medium is usually small compared to the diameter of the detector ring. The second method is the use of a pulse-height threshold that rejects scattered photons with an energy below E_p. In single Compton scattering this corresponds to a maximum scattering angle θ_p (see Ref. *22*, Eq. 8e–5), where

$$\cos(\theta_p) = 2 - \frac{511 \text{ keV}}{E_p} \quad (3)$$

For scattered coincident events the effective maximum scattering angle θ_m is the smaller of θ_f and θ_p. (For single counts the maximum scattering angle is always θ_p.) The effective minimum scattered gamma energy E_m corresponding to θ_m is given by:

$$E_m = \frac{511 \text{ keV}}{2 - \cos(\theta_m)} \quad (4)$$

Where only one member of the annihilation pair scatters, the rate of scattered coincident events is approximated by:

$$C_1 = \left[\frac{\rho a S c}{T}\right]\left[\frac{S(1 - P_s)}{c}\right]\left[\frac{P_s g_1 S}{c}\right]\left[\epsilon\epsilon_m\right] = \frac{\rho a S^3 g_1 \epsilon\epsilon_m P_s(1 - P_s)}{Tc}, \quad (5)$$

where $P_s = 1 - e^{-\mu L/2}$, the probability a 511-keV photon will scatter on passing through half the tissue; ϵ_m is the average detection efficiency for photons between energy E_m and 511 keV; and g_1 is a solid-angle factor. The first bracket is the contributing activity; the second bracket is the probability that either photon reaches a detector without scattering; the third bracket is the probability that the other photon scatters and reaches one of the opposing (coincident) detectors; and the fourth bracket is the probability that both photons are detected and pass the pulse-height threshold. This expression assumes that the activity is near the center of the scattering medium, that the scattering takes place close to the axis of the ring, and that single scattering predominates.

The dimensionless quantity g_1 describes the fraction of Compton scattering angles that fall within the angular strip S/c wide and $2\theta_m$ long:

$$g_1 = \frac{\int_{-\theta_m}^{\theta_m} \frac{d\sigma}{d\Omega} d\theta}{\int_0^{\pi} 2\pi \frac{d\sigma}{d\Omega} \sin\theta \, d\theta}, \quad (6)$$

where $d\sigma/d\Omega$ is the collision differential cross section for Compton scattering of 511-keV photons on free electrons, given by the Klein–Nishina formula (see Ref. *22*, Eq. 8e–13).

The rate of scattered coincident events C_2, where both members of the annihilation pair have scattered, is approximated by:

$$C_2 = \left[\frac{\rho a S c}{T}\right]\left[\frac{SP_s}{2c}\right]\left[\frac{P_s g_2 S}{c}\right]\left[\epsilon_m^2\right] = \frac{\rho a S^3 g_2 \epsilon_m^2 P_s^2}{2Tc}, \quad (7)$$

where g_2 is an appropriate solid-angle factor defined similarly to g_1. (See Ref. *18* for details.)

Note that the backgrounds C_1 and C_2 are not associated with time resolution but with scatter geometry and energy resolution. As expected, the ratio of scattered coincident events ($C_1 + C_2$) to unscattered coincident events (C_0) is lowest for "good scatter geometry" (i.e., small S/T).

The single counting rate C_s is given by:

$$C_s = \left[\frac{2\rho a S c}{T}\right]\left[\frac{S}{2c}\right]\left[\epsilon(1 - P_s) + \epsilon_p P_p\right] = \frac{\rho a S^2}{T}\left[\epsilon(1 - P_s) + \epsilon_p P_p\right], \quad (8)$$

where P_p is the probability that a photon will scatter in tissue and retain an energy greater than E_p (i.e., the pulse-height threshold) and ϵ_p is the average detection efficiency for such photons. We may approximate:

$$P_p = P_s\left(\frac{511 \text{ keV} - E_p}{341 \text{ keV}}\right) \text{ for } E_p \geq 170 \text{ keV}$$
$$\text{and } P_p = Ps \text{ for } E_p < 170 \text{ keV}. \quad (9)$$

The accidental coincidence rate C_a is given by:

$$C_a = fC_s^2 t, \quad (10)$$

where t is the time resolution. It is of importance to calculate the maximum rate $\hat{C}_0$ for a certain fraction $\eta = C_a/C_0$ of accidental coincidences:

$$\hat{C}_0 = \frac{\eta T^2 \epsilon^4 (1 - P_s)^4}{16 \, ftc^2 [\epsilon(1 - P_s) + \epsilon_p P_p]^2}. \quad (11)$$

As expected, the maximum event rate is enhanced by good time resolution, good shielding, and good detection efficiency. It is important to reduce f to the point where all (or almost all) of the activity lies within the radius R (Eq. 2). Reducing f below this value will reduce the signal C_0 approximately as f^2 (without affecting the single counting rate C_s) and will actually cause $\hat{C}_0$ to decrease.

For the example of Case 2 in Table 1 and for a 10% accidental coincidence rate ($\eta = 0.10$) we have:

$$\hat{C}_0 = 6{,}990 \text{ events/sec}$$

and

$$\rho = 305 \ \mu\text{Ci/axial cm.}$$

The profound effect that the scattering medium has on the maximum event rate can be seen by noting what these values would be in the absence of the scattering medium (i.e., $P_s = P_p = 0$):

$$\hat{C}_0 = 130{,}000 \text{ events/sec}$$

and

$$\rho = 780 \ \mu\text{Ci/axial cm.}$$

One should note that (A) increasing T (whenever possible) by extending the shielding closer to the patient reduces all backgrounds without reducing the sensitivity; (B) increasing the section thickness S increases the sensitivity as S^2 but the scattered coincident background increases as S^3; and (C) the maximum event rate $\hat{C}_0$ (as limited by accidentals) is not a function of S.

DEADTIME

Deadtime arises from the limited speed of both the scintillation process and the electronic circuits. After the interaction of a photon in NaI(Tl), 800 nsec are required to collect 90% of the available scintillation light (91% of the light is emitted with an exponential time constant of 218 nsec and 9% is emitted with an exponential time constant of 1,340 nsec) (*23*). To preserve pulse-height information to within 10% at high counting rates it is therefore necessary to reject all counts that occur within approximately 800 nsec of another count. This requirement results in a paralyzing deadtime of 800 nsec for each coded segment of the ring. The circuits that perform the pulse-height selection may also introduce a paralyzing deadtime, but by proper design (*24*) it is possible to limit the overall paralyzing deadtime t_p to 1 μsec. The circuits that handle the time coincidence and position information introduce a nonparalyzing deadtime t_n of $\leq$200 nsec, but this does not result in an appreciable loss of counts, provided the circuits are properly designed and $t_n \leq t_p$.

In Cases 2 and 3 of Table 1, where a pulse-height selection is imposed, the fraction of time that each 36-crystal segment is available is e^{-Gt_p}, and the fraction of counts f_c lost per segment is given by:

$$f = 1 - e^{-Gt_p}. \quad (12)$$

G is the gross counting rate for each segment (1.3×10^5), $t_p = 1$ μsec, and the fraction of counts lost (f_c) is 12%. As a coincident event requires that two segments be available for counting (probability = e^{-2Gt_p}), the fraction of coincident events lost (f_e) is given by:

$$f_e = 1 - e^{-2Gt_p} \quad (13)$$

and equals 23% for this example.

In Case 1 of Table 1 no pulse-height selection is imposed and we assume that the paralyzing dead-time can be reduced to 200 nsec. In this case the fraction of counts lost (f_c) is 2.5% and the fraction of events lost (f_e) is only 5%, but the backgrounds are larger (see Table 1).

RECONSTRUCTION METHODS

For the ring detector system of densely packed crystals presented in this analysis, each of the 288 crystals is in coincidence with 62 opposing crystals, providing 8,928 crystal pair combinations. Four possible methods of reconstruction are envisioned (for reviews of reconstruction techniques see Refs. *5* and *6*). The first method is to generate a back-projection image from the distribution of lines connecting coincident detector pairs. Reconstruction is accomplished using two-dimensional Fourier transform techniques. The second method is to store the lines connecting coincident detector pairs into bins corresponding to intervals of direction and position. The data are then reconstructed using the algorithm of back projection of filtered projections. The third method is to multiply either the back-projection image or the binned data by the generalized pseudo-inverse matrix, which has been derived for the particular geometry of the system. The fourth method is the use of the closed-form expressions of Marr that permit the activity distribution to be estimated directly from a list of the coincident detector pairs (*25*).

ATTENUATION CORRECTIONS

Although the corrections for attenuation are much smaller for coincident annihilation imaging than for single gamma imaging, some correction is needed to obtain good transaxial reconstructions. One possibility is the use of a continuous source of positron emitter around the outside of the patient, as suggested by Phelps, et al (*3*). Since the attenuation depends only on the line of flight of the two photons, and not on the position of the point of annihilation, the attenuation correction for each pair of coincident detectors is the ratio of the transmitted flux before and after the patient is positioned in the system.

A second possibility is the use of a fan beam source of 7.8-yr ^{133}Ba (principal gamma energy 356 keV) that travels 180 deg around the patient while the opposing 62 crystals collect transmission data. As the attenuation cross section is greater at 356 keV than at 511 keV by a factor of 1.16 for water, muscle, and bone (*26*), the attenuation correction for 511-keV pairs is determined as the 0.86 power of the ratio of the transmitted flux of 356-keV photons before and after the patient is positioned in the system. It is necessary to know the attenuation to an accuracy of only 10% rather than the 1% accuracy of the EMI scanner, and approximately 100 times fewer counts are needed. Thus the dose is reduced from 1–3 rads to 50–150 mrads. This second method permits greater ease of source collimation to reduce patient exposure, greater data rates, and the use of an emitter of long half-life.

In summary, we have presented an analysis of the potentials and limitations of a new scheme for the high-resolution imaging of positron-emitting pharmaceuticals in nuclear medicine. With an activity density of 200 μCi/cm (typically 5–20 mCi in the patient) and an energy resolution of 30% FWHM the device should operate at 7,000 events/sec. Seventy percent of these are useful unscattered coincident events, 25% are scattered coincident background, and 5% are accidental coincident background. The device can operate at two to three times higher event rates with increased backgrounds.

In conventional dynamic scintigraphy the quantitative assessment of regional brain blood flow is severely limited by the fact that the volume of interest is unknown (*27*). This system has the speed capability (~5,000 counts/1-sec frame) for assessment of blood flow in relatively large but well-defined volumes ($4 \times 4 \times 1$ cm) using $^{13}NH_4^+$, $^{68}Ga^+$, $^{82}Rb^+$, and ^{11}C or ^{15}O on appropriate compounds. For gated studies of the myocardial uptake of nuclides [e.g., ^{82}Rb (*28*), ^{13}N-ammonia, or ^{13}N-labeled-L-asparagine (*29*)] the system will give images with 4–6 mm resolution (FWHM).

ACKNOWLEDGMENTS

We thank L. W. Alvarez for his encouragement and suggestions. This work was supported in part by NIH Grant 1 R01 GM-20115-02 RAD and in part by the U.S. Energy Research and Development Administration.

REFERENCES

1. RANKOWITZ S, ROBERTSON JS, HIGINBOTHAM WA, et al: Positron scanner for locating brain tumors. *IRE Int Conv Record* 10(9): 49–56, 1962

2. ROBERTSON JS, MARR RB, ROSENBLUM M, et al: 32 crystal positron transverse section detector. In *Tomographic Imaging in Nuclear Medicine*, Freedman GS, ed, New York, Society of Nuclear Medicine, 1973, pp 142–153

3. PHELPS ME, HOFFMAN EJ, MULLANI NA, et al: Application of annihilation coincidence detection to transaxial reconstruction tomography. *J Nucl Med* 16: 210–224, 1975

4. TER-POGOSSIAN MM, PHELPS ME, HOFFMAN EJ, et al: A positron-emission transaxial tomograph for nuclear imaging (PETT). *Radiology* 114: 89–98, 1975

5. GORDON R, HERMAN GT: Three dimensional reconstruction from projections: a review of algorithms. *Int Rev Cytol* 38: 111–151, 1974

6. BUDINGER TF, GULLBERG GT: Three-dimensional reconstruction in nuclear medicine emission imaging. *IEEE Trans* 21(3): 2–20, 1974

7. GLASS HI: New applications of radiopharmaceuticals labeled with cyclotron-produced radionuclides. In *Medical Radioisotope Scintigraphy*, vol 2, Vienna, IAEA, 1972, pp 299–324

8. SILVESTER DJ, CLARK JC, PALMER AJ: The future of accelerator-produced radiopharmaceuticals. In *Proceedings of First World Congress of Nuclear Medicine*, Tokyo, Sept 30–Oct 4, 1974, pp 181–190

9. SUBRAMANIAN G, RHODES BA, COOPER JF, et al, eds: *Radiopharmaceuticals*, New York, Society of Nuclear Medicine, 1975: to be published

10. WRENN FR, GOOD ML, HANDLER P: The use of positron-emitting radioisotopes for the localization of brain tumors. *Science* 113: 525–527, 1951

11. BROWNELL GL, SWEET WH: Localization of brain tumors. *Nucleonics* 11: No. 11, 40–45, 1953

12. ANGER HO: Survey of radioisotope cameras. *Instrum Soc Am Trans* 5: 311–334, 1966

13. BURNHAM CA, BROWNELL GL: A multi-crystal positron camera, *IEEE Trans* 19(3): 201–205, 1972

14. LIM CB, CHU D, KAUFMAN L, et al: Initial characterization of a multiwire proportional chamber positron camera, *IEEE Trans Nucl Sci* 22: No 1, 388–394, 1975

15. MUEHLLEHNER G: Positron camera with extended counting rate capability. *J Nucl Med* 16: 653–657, 1975

16. JONES T, BROWNELL GL, TER-POGOSSIAN MM: "Equilibrium" images of short-lived radiopharmaceuticals for dynamic observations. *J Nucl Med* 15: 505, 1974

17. CHO ZH, ERIKSSON L, CHAN J: A circular ring transverse axial positron camera. Presented at the Workshop on Reconstruction Tomography in Diagnostic Radiology and Nuclear Medicine, Puerto Rico, April, 1975

18. DERENZO SD, ZAKLAD H, BUDINGER TF: *Positron Emission Camera for Transverse Section Tomography*. Lawrence Berkeley Laboratory Report No LBL-2848, 1975 (unpublished)

19. ALVAREZ LW: *A new γ-ray imaging camera*. Group A Physics Note No 784, May 1974, available from Group A, Lawrence Berkeley Laboratory, Berkeley Calif 94720 (unpublished)

20. GRENIER RP, BENDER MA, JONES RH: A computerized multi-crystal scintillation gamma camera. In *Instrumentation in Nuclear Medicine*, vol 2, Hine GJ, Sorenson JA, eds, New York, Academic Press, 1974

21. BRAUNSFURTH J, KÖRNER HJ: Zeitauflösungseigenschaften von NaJszintillatoren. *Nucl Instrum Meth* 34: 202–212, 1965

22. GRAY DE, ed: *American Institute of Physics Handbook*, 3rd ed, New York, McGraw-Hill, 1972

23. TIDD JL, DABBS JR, LEVINE N: *Scintillator Handbook with Emphasis on Cesium Iodide*, NASA Technical Memorandum No NASA TM-X-64741, April 1973, available from the National Technical Information Service, Springfield, Va 22151 (unpublished)

24. BLATT SL, MAHIEUX J, KOHLER D: Elimination of pulse pileup distortion in nuclear radiation spectra. *Nucl Instrum Meth* 60: 221–230, 1968

25. MARR RB: On the reconstruction of a function on a circular domain from a sampling of its line integrals. *J Math Anal Appl* 45: 357–374, 1974

26. HUBBELL JH: *Photon Cross Sections, Attenuation Coefficients, and Energy Absorption Coefficients from 10 keV to 100 GeV*, US National Bureau of Standards Report NSRDS-NBS 29, 1969

27. BUDINGER TF, DELAND FH, DUGGAN HE, et al: Dynamic time-dependent analysis and static three-dimensional imaging procedures for computer assisted CNS studies. In *Past, Present, and Future of Noninvasive Brain Imaging*, DeBlanc HJ, Sorenson T, eds, New York, Society of Nuclear Medicine, 1975: to be published

28. BUDINGER TF, YANO Y, HOOP B: A comparison of $^{82}Rb^{+}$ and $^{13}NH_3$ for myocardial positron scintigraphy. *J Nucl Med* 16: 429–431, 1975

29. GELBARD AS, CLARKE LP, LAUGHLIN JS: Enzymatic synthesis and use of ^{13}N-labeled L-asparagine for myocardial imaging. *J Nucl Med* 15: 1223–1225, 1974